https://doi.org/10.1016/j.msea.2019.138695

Achieving stable plastic flows in a Zr-based bulk metallic glass under tailored mixed-mode (I/II) loading conditions

S.H. Chen[1,2*], H.H. Tang[1], H.M. Zheng[1], W.J. Chang[1], J.C. Zhang[1], H.D. Yang[1], Z.F. Zhang[1], D.B. Yu[3], K.C. Chan[4] and R.P. Liu[2*]

[1]School of Mechanical Engineering, Hefei University of Technology, Hefei 230009, China.

[2]State Key Laboratory of Metastable Materials Science and Technology, Yanshan University, Qinhuangdao 066004, China

[3]School of Materials Science and Engineering, Hefei University of Technology, Hefei 230009, China.

[4]Advanced Manufacturing Technology Research Centre, Department of Industrial and Systems Engineering, The Hong Kong Polytechnic University, Hung Hom, Kowloon, Hong Kong.

* Corresponding author. shchen@hfut.edu.cn (S.H. Chen) & riping@ysu.edu.cn (R.P. Liu).

Abstract

The achievement of stable plastic flows plays a key role for practical structural applications of bulk metallic glasses (BMGs). In this work, by designing complex stress fields through tailored double-side notches, stable plastic flows in a Zr-based BMG were achieved under mixed-mode (I/II) loading conditions. The deformation behavior of the notched BMG specimens, including the shear-banding and fracture behaviors, was examined and correlated to the designed complex stress fields. The findings have shown that the stable plastic flows were mainly caused by the introducing of mode-II component under the mixed-mode (I/II) loading conditions. Increase of the mode-II component can result in not only more stable plastic flows, but also larger bearing loads. The present findings are of significance in uncovering the plastic deformation mechanisms of BMGs under mixed-mode loading conditions and in designing BMG structures with better mechanical performance.

Key words: Bulk metallic glass; Plastic flow; Mixed-mode; Complex stress field; Shear band.

1. Introduction

With unique mechanical properties, such as a relatively large elasticity of about 2%, high strength and high hardness, bulk metallic glasses (BMGs) are considered as being poised for wide-spread structural-applications [1,2]. However, the brittle nature of BMGs at room temperature has significantly hindered the practical applications of BMGs in industry [3,4]. The achievement of stable plastic flows in BMGs is important, not only for elucidating the plastic-flow mechanisms, but also for the application of BMG structures/components with better mechanical performance. Although stable plastic flows of BMGs in compressive tests have been widely achieved by techniques such as the adjusting of compositions [5,6], introducing of externally geometric confinement [7,8], and surface treatment [9,10], how to achieve stable plastic flows in BMGs under tensile or mixed-mode loading conditions are still very challenging. Fortunately, in practical applications of structural materials (including BMGs and BMG structures), they always deform under mixed-mode loading conditions or complex stress fields, rather than the relatively-uniform stress distributions occurring during pure tension/compression tests [11-15]. With presence of complex stress fields, BMGs and BMG structures have good potential for achieving large plastic flows [16-18]. Research has also demonstrated that BMGs can display tunable shear-banding behavior as well as plastic deformation under mixed-mode loading conditions [19-23]. This suggests that although BMGs are brittle in nature, BMG structures may still demonstrate plastic deformation behavior in practical applications. By creating complex stress fields through the introducing of double-side notches, Qu et al. [24,25] achieved some flow serrations in tensile BMG specimens, suggesting that the introducing of double-side notches may be useful for achieving stable plastic flows under tensile loading. Thereafter, Chen et al. [16,22] have further designed some notched BMG specimens in the presence of complex stress fields (under mixed-mode loading conditions), and obtained a wide range of stable plastic flows. Although previous studies have focused on the plastic deformation behavior of BMGs under mixed-mode loading conditions [16,19-23], these studies focused on the formation and propagation of shear bands as well as

plastic-flow dynamics. The mechanisms on how to achieve stable plastic flows in notched BMG specimens under mixed-mode loading conditions is still unknown. In this work, with the aim of uncovering the mechanisms on how to achieve stable plastic flows under mixed-mode loading conditions, more specimens with varying mode mixities were designed and investigated. The findings have demonstrated that the achievement of stable plastic flows can be attributed to the introducing of the mode-II component. Moreover, a relatively higher bearing load can also be obtained by increasing the mode-II component. The present findings give additional insight into the plastic-flow mechanisms of BMGs, and provide guidance on the design of BMG structures with better plastic deformation performance.

2. Methods

As-cast $Zr_{57}Cu_{20}Al_{10}Ni_8Ti_5$ (at.%) BMG rods, of 3 mm diameter, were produced by suction-casting the melted mixture of pure raw materials into water-cooled copper molds. In order to achieve stable plastic flows, three groups of notched specimens with tailored mixed-mode (I/II) loading conditions were designed, as shown in Fig. 1. The mode mixities (I/II) of the notched specimens can be determined by the equation $M^e = (2/\pi)\tan^{-1}(\sigma_n/\tau)$ [22,23], where M^e = 1 and 0 correspond to pure mode-I and mode-II, respectively. In this work, since some of the specimens deform under more complex situations, for example, the presence of bending moment in group **L** specimens, half-quantitative determinations of the mode mxities were used to study the effect of mode mixities on the plastic-flow behavior of the notched specimens. Under applied loadings, the specimen **R0** deforms under a pure mode-I loading condition. With increase of parameter *b*, the other group **R** specimens (**R1**, **R2** and **R3**) tend to deform under mixed-mode (I/II) loading conditions, and a larger *b* value leads to a higher mode-II component. The group **M** specimens also deform under a mixed-mode (I/II) loading condition, where the mode-II component plays a predominant role [22]. For group **L** specimens, besides the mixed-mode (I/II) loading condition, the negative parameter *a* causes a bending moment that acts on the shear plane [16]. The increase of parameter *b* also results in an increase of the mode-II

component in both groups of **M** and **L** specimens. To better describe the specimens with varying mode mixities, the three groups of specimens were annoted as a mixed-mode (group **R**), predominantly-mode-II (group **M**), and mixed-mode+bending (group **L**), respectively. These specimens (**R**, **M**, **L**) with varying geometrical parameters (*a*, *b*) were then fabricated from the as-cast rods by electrical discharge machining (EDM). The machined surfaces were polished to a mirror finish using abrasive papers for shear-banding observations. The mechanical tests were conducted on an Instron 5565 materials testing machine with a displacement-loading rate of 0.06 mm/min, and for each condition, three specimens were tested for repeatability. The load-axial displacement curves were recorded at 100 points per second. After mechanical testing, the specimens were inspected using scanning electron microscopy (SEM).

3. Results

3.1 Plastic flows

It is known that the room-temperature plastic deformation of BMGs is accommodated by the initiation of shear bands, displaying serrated flows in the loading-displacement or stress-strain curves [26-29]. These flow serrations are therefore investigated inversely in many previous studies to give more insight into the plastic deformation mechanisms of BMGs [30-38]. As shown in Fig. 2a, for the **R0** specimen with a pure mode-I loading condition, several flow serrations were obtained. As compared with the $Zr_{57}Cu_{20}Al_{10}Ni_8Ti_5$ (at.%) BMG specimens without notches [39], the introducing of double-side notches significantly improved the formation of shear bands around the notch root. Since the formation of shear bands in double-side-notched BMG specimens has been examined in previous studies [24] and the specimen **R0** was mainly used for comparison here, the formation of shear bands and flow serrations in the **R0** specimen are not discussed in detail in this work. For the other specimens with mixed-mode (I/II) loading conditions (**R1**-**R3**, **M1**-**M3**, and **L1**-**L3**), the plateau stages of serrated plastic flows were observed, and an example of the **M3** specimen is indicated in Fig. 2b. The observation of more plastic flows indicates that during the

loading process, more shear bands were initiated, and the specimens were deformed more plastically. More importantly, as compared with the **R0** specimen where the plastic-flow curve decreased rapidly after peaking, these plateau stages suggest that the specimens have undergone stable plastic flows under applied loadings. In order to further characterize the plastic flows of these specimens, the axial displacements with flow serrations (d_p) and plateaus (d_s), were collected, denoting the plastic-flow stage and stable plastic-flow stages, respectively. The plastic-flow stages were calculated from the displacement point at which the first load drop (Δf) larger than 0.15 N occurred [16], as indicated in Fig. 2d, to the failure point.

The detailed d_p and d_s values are given in Fig. 3. It can be seen that the **R0** specimen has the smallest d_p (0.0262 ± 0.0049 mm) and d_s (0.0030 ± 0.0018 mm) values, while the other specimens with mixed-mode (I/II) loading conditions have more plastic flows. The three groups of specimens (groups **R**, **M** and **L**) have demonstrated varying effects on the initiation of plastic flows. For example, for the same parameter b = 0.4 mm, the **R1**, **M1** and **L1** specimens have d_p values of 0.0446 ± 0.0008, 0.0715 ± 0.0176, and 0.1889 ± 0.0189, respectively. This suggests that the formation of plastic flows is not only dependent on the mixed-mode (I/II) loading conditions, but is also affected by the mode mixities. For the **R1** specimen, both the mode-I and mode-II components play roughly equivalent roles during the loading process; while for the **M1** specimen, it is clear that the mode-II component plays a more dominant role [22]; and for the **L1** specimen, the negative a value results in a bending moment acting on the shear plane, and the specimens deform under a more complex stress state [16]. Nevertheless, for all groups of specimens (**R**, **M**, and **L**), the increase of the mode-II component by increasing the parameter b can result in the formation of more plastic flows (Fig. 3a). The formation of stable plastic flows (d_s) also shows similar trends to the plastic flow values (d_p), as given in Fig. 3b. The present findings suggest that more plastic flows can be achieved by tuning the mode mixity of the mixed-mode (I/II) loading conditions. The **M3** specimen has the largest plastic flow stage width of 0.1889 ± 0.0189 mm, and a stable plateau stage width of 0.0799 ± 0.026 mm. With

the introducing of a bending moment, the **L3** specimens even have larger d_p and d_s values of 0.562 ± 0.1822 and 0.1851 ± 0.0314 mm, respectively. As compared with a notch distance of 0.8 mm (i.e., the parameter *b*), the large axial displacements suggest the occurrence of large plastic deformation in localized regions between two notches, which is still impressive for a BMG and could be useful for the design of BMG structures with better plastic deformation performance.

3.2 Bearing load

For the engineering application of structural materials, besides the property of plasticity, strength also plays a significant role. Usually, for natural materials, the plasticity and strength are mutually exclusive [40]. However, in this work, it was interesting to find that with the increase of plastic flows, the bearing load of the specimens also increased, as shown in Fig. 2. In order to better compare the load-bearing capacity of the notched specimens, normalized stress was also calculated by $\sigma_N = F/(n_{max}t)$, where F is the bearing load, n_{max} is the maximum absolute value of the parameter a, and t is the thickness. To characterize the bearing load of these specimens, the load at which the first load drop larger than 0.15 N occurs is defined as the "yield" load, F_y. The "yield" load data of the notched specimens are shown in Fig. 4a. It can be seen that, at a certain parameter b (for example, b = 0.4 mm), the group **R** specimens (**R1**) have the largest bearing load, and the group **L** specimens (**L1**) have the smallest value. As compared with the group **R** specimens, the increase in plastic flows in groups **M** and **L** specimens was achieved by scarifying the bearing load, especially for the group **L** specimens. However, with the increasing of parameter b, it is interesting to find that all groups of specimens (**R**, **M** and **L**) tend have increased bearing loads (F_y). This implies that with the increase of the mode-II component, the failure process can therefore be delayed to afford larger loads. For each group of specimens, the increase of the mode-II component can simultaneously improve both the plastic flows (d_p) and bearing loads (F_y). Typically, for the group **R** specimens, the specimens under the mixed-mode loading condition have a much larger "yielding" load (the average F_y = 345 N, 378 N, and 460 N, for **R1**, **R2** and **R3** specimens,

respectively.) than the one under the pure-mode-I loading condition (the average F_y = 305 N for the **R0** specimen). The findings suggest that the change of loading condition from a pure mode-I to mixed-mode (I/II) can also enhance the bearing load. The maximum load of these notched specimens, noted as F_m, is shown in Fig. 4b. The maximum loads (F_m) of these specimens with mixed-mode loading conditions also show similar trends to the "yield" load (F_y). This has further confirmed the improvement in bearing loads, where for group L specimens, the maximum load (F_m) has even been enhanced more significantly than the "yield" load (F_y).

4. Discussion

The plastic-flow serrations are correlated to the formation and propagation of shear bands [27]. In order to uncover the plastic deformation mechanisms, the formation of shear bands of the designed specimens was inspected in the deformed specimens before failure. The formation of the shear bands of group **R** specimens is given in Fig. 5. The **R1** specimen has circumferential shear bands distributed between the notch bottoms (Fig. 5a), which are highly in line with the double-side-notched specimens in a previous work [24]. While for the other group **R** specimens, due to the increase of parameter *b*, the formation of the shear bands is changed accordingly. Firstly, some circumferential shear bands are observed, emanating from the notch bottoms, as can be seen in Fig. 5b, c and e. However, these circumferential shear bands can only trigger the formation of serrations with relatively-smaller load drops, which cannot result in the final fracture of the specimens [16,22]. Secondly, besides the formation of circumferential shear bands, some shear bands were observed between the notch bottoms, noted as primary shear bands (primary SB, as indicated in Fig. 5b, d and f). The sliding of the primary shear band accommodates the stable plastic flows, and results in a shear offset at the notch bottom (Fig. 5c) [22]. With the increase of parameter *b*, the **R2** and **R3** specimens tend to have more primary shear bands with larger shear-banding angles. A typical **R3** specimen is given in Fig. 5d, where more primary shear bands can be observed, together with a larger shear offset at the notch root (Fig. 5e). The shear-banding angles of the primary shear band have also changed

from 46° in the **R1** specimen to 57° in the **R3** specimen. Besides the primary shear bands, some secondary shear bands between the primary shear bands were also observed. This can further increase the formation of more stable plastic flows. The achievement of the stable plastic flows in group **R** specimens with increase of the mode-II component can be concluded as resulting from the initiation of more primary shear bands with larger shear-banding angles and multiple secondary shear bands between them.

In group **M** specimens with larger mode-II components, more primary shear bands were observed, as shown in a typical **M1** specimen in Fig. 6a. As compared with the **R1** specimen, the **M1** specimen not only has more primary shear bands (Fig. 6c), but also demonstrates more shear offsets at the notch root (Fig. 6b). With increase of the parameter *b*, group **M** specimens have shown a similar trend to group **R** specimens, where more primary and secondary shear bands were observed. In group **L** specimens, with a bending moment, the shear banding angles has been deflected significantly, which suggests that the propagation of shear bands has been impeded, where more plastic flows occurred, resulting in the formation of a larger shear offset with a curved shear-banding plane, as shown in Fig. 6e. Besides more primary shear bands, a large number of secondary shear bands were initiated in the regions between the notches, agreeing well with the formation of more plastic flows. With the increase of parameter *b*, similar trends in the formation of primary and secondary shear bands were also found in these group **L** specimens. These findings have further confirmed the above-mentioned conclusion that the formation of more stable plastic flows can be related to the initiation of more primary shear bands and multiple secondary shear bands between the primary shear bands.

To characterize the bearing load of different groups of specimens, the fracture process of these specimens was further examined. For the **R0** specimen, a large number of circumferential shear bands (Fig. 5a) were formed within the stress-concentrated regions, where the complex stress fields not only cause the formation of more shear

bands, but also a relatively lower bearing load (310 N). While for **R1** specimen (Fig. 5b), the fracture plane has been confined by the designed complex stress fields, and it is expected that the specimen will fracture along the direction of the primary shear band. Thus, the shear-banding angles of the primary shear band can also be noted as fracture-plane angles, i.e., α = 46°, for the **R1** specimen. The increase of parameter *b* results in the increase of the fracture-plane angles to 51° in the **R2** specimen, and 57° (Fig. 5d) for the **R3** specimen. Studies on the fracture behavior of a Zr-based BMG with similar composition ($Zr_{52.5}Cu_{17.9}Ni_{14.6}Al_{10}Ti_5$, *at*.%) has shown that the fracture behavior of such a BMG may follow an Ellipse criterion, and the increase of the fracture-plane angles can result in a larger bearing load [37]. For group **M** specimens under predominantly-mode-II loading conditions, the increase of the mode-II component also result in the increased fracture-plane angles (68°, 76° and 77° for **M1**, **M2** and **M3** specimens, respectively). While for the group **L** specimens, due to the introducing of bending moment, the primary shear-banding angles were varying during the loading process (Fig. 6f), and the fracture plane was also deflected (Fig. 6d). The fracture process cannot be determined using the Ellipse criterion. Nevertheless, the shear-banding angles of the group **L** specimens were collected, as ranging from 75° to 82°, and the range is similar for all groups of specimens. With similar fracture-plane angles, the enhancement of the bearing load in group **L** specimens can be attributed to the enlargement of the fracture-plane areas.

In this work, we have shown that by appropriate design of mixed-mode (I/II) loading conditions, the notched BMG specimens tend to have more plastic flows, including stable plastic-flow-plateaus, and increased bearing loads. The increase in the more plastic flows can be attributed to the initiation of more primary shear bands with varied shear-banding angles and multiple secondary shear bands between them, resulting from the increase of the mode-II component. On the other hand, although the different groups of specimens (**R**, **M** and **L**) demonstrate varying load-bearing capacity on the change of the mixture of loading conditions, the increasing of bearing loads in each group of specimens can be attributed to the increasing of the

fracture-plane angles as well as the enlargement of the fracture-plane areas, which is also caused by the increase of the mode-II component. Therefore, it can be concluded that the tuning of mode-II component could be a key to achieving more plastic flows as well as larger bearing loads in the BMGs under mixed-mode (I/II) loading conditions. As indicated in Fig. 7, it can be seen that all groups of specimens tend to have better combinations of plastic flows and bearing loads with the increase of the mode-II component. The present work gives greater insight into the plastic deformation mechanisms of BMGs under complex stress fields/mixed-mode (I/II) loading conditions. Since the shear-banding mechanisms in BMGs are still under debate [42], the present findings can be used to design MG specimens with tailored plastic flows in order to investigate the initiation and propagation of shear bands. For example, the initiation and propagation of shear bands was significantly affected by the surface roughness [43], where the design of nanoscaled complex stress fields in specimens/on the sample surfaces could be used to shed more light on the shear-banding mechanisms in MGs. Additionally, the BMG structures have demonstrated great potential for mechanical energy absorption under compressive loadings, and high elastic performance under tensile loadings [15,18,44,45]. The present findings suggest that under tensile loading, the BMG structures may also have the capability to deform plastically. The design of BMG structures by tuning the mode-II component may demonstrate better mechanical performance in practical structural applications.

5. Conclusions

Three groups of notched BMG specimens with varying mode mixities were designed and investigated. Stable plastic flows were achieved in the specimens under mixed-mode (I/II) loading conditions, and were mainly attributed to the introducing of the mode-II component. For all groups of specimens, the increase of the mode-II component can result in the formation of more shear bands and the change of shear-banding angles, leading to more plastic flows as well as larger bearing loads. The present findings are significant in understanding the plastic deformation

mechanisms of BMGs and in designing of BMG structures with better mechanical performance for practical structural-applications.

Acknowledgements

The work described in this paper was supported by grants from the National Natural Science Foundation of China under research project No. 51801049 and 21606217, and a grant from the State Key Laboratory of Metastable Materials Science and Technology, Yanshan University (project No. 201809). This work was also supported by the Fundamental Research Funds for the Central Universities of China (Grant No. PA2019GDZC0096).

Declarations of interest: The authors declare no conflict of interest.

Data Availability

The raw/processed data will be made available on request.

References

[1] J. Plummer, W.L. Johnson, Is metallic glass poised to come of age?, Nat. Mater. 14 (2015) 553-555.

[2] Z. Liu, W. Chen, J. Carstensen, J. Ketkaew, R.M.O. Mota, J.K. Guest, J. Schroers, 3D metallic glass cellular structures, Acta Mater. 105 (2016) 35-43.

[3] M.M. Trexler, N.N. Thadhani, Mechanical properties of bulk metallic glasses, Prog. Mater. Sci. 55 (2010) 759-839.

[4] B.A. Sun, W.H. Wang, The fracture of bulk metallic glasses, Prog. Mater. Sci. 74 (2015) 211-307.

[5] Y.H. Liu, G. Wang, R.J. Wang, D.Q. Zhao, M.X. Pan, W.H. Wang, Super plastic bulk metallic glasses at room temperature, Science 315 (2007) 1385-1388.

[6] S.F. Guo, J.L. Qiu, P. Yu, S.H. Xie, W. Chen, Fe-based bulk metallic glasses: Brittle or ductile?, Appl. Phys. Lett. 105 (2014) 161901.

[7] W. Chen, K.C. Chan, S.F. Guo, P. Yu, Plasticity improvement of an Fe-based bulk metallic glass by geometric confinement, Mater. Lett. 65 (2011) 1172-1175.

[8] W. Chen, K.C. Chan, S.H. Chen, S.F. Guo, W.H. Li, G. Wang, Plasticity enhancement of a Zr-based bulk metallic glass by an electroplated Cu/Ni bilayered coating, Mater. Sci. Eng. A 552 (2012) 199-203.

[9] C. Ma, S. Suslov, C. Ye, Y.L. Dong, Improving plasticity of metallic glass by electropulsing-assisted surface severe plastic deformation, Mater. Des. 165 (2019).

[10] G.J. Wu, R. Li, Z.Q. Liu, B.Q. Chen, Y. Li, Y. Cai, T. Zhang, Induced multiple heterogeneities and related plastic improvement by laser surface treatment in CuZr-based bulk metallic glass, Intermetallics 24 (2012) 50-55.

[11] G. Kumar, A. Desai, J. Schroers, Bulk metallic glass: The smaller the better, Adv. Mater. 23 (2011) 461-476.

[12] S.H. Chen, J.Y. Wang, L. Xia, Y.C. Wu, Deformation behavior of bulk metallic glasses and high entropy alloys under complex stress fields: A review, Entropy 21 (2019) 54.

[13] M. Jafary-Zadeh, G.P. Kumar, P.S. Branicio, M. Seifi, J.J. Lewandowski, F. Cui, A critical review on metallic glasses as structural materials for cardiovascular stent applications, J. Funct. Biomater. 9 (2018) 19.

[14] M.M. Khan, A. Nemati, Z.U. Rahman, U.H. Shah, H. Asgar, W. Haider, Recent advancements in bulk metallic glasses and their applications: A review, Crit. Rev. Solid State 43 (2018) 233-268.

[15] S.H. Chen, K.C. Chan, T.M. Yue, F.F. Wu, Highly stretchable kirigami metallic glass structures with ultra-small strain energy loss, Scr. Mater. 142 (2018) 83-87.

[16] S.H. Chen, K.C. Chan, G. Wang, F.F. Wu, L. Xia, J.L. Ren, J. Li, K.A. Dahmen, P.K. Liaw, Loading-rate-independent delay of catastrophic avalanches in a bulk metallic glass, Sci. Rep. 6 (2016) 21967.

[17] L.Y. Chen, Q. Ge, S. Qu, Q.K. Jiang, X.P. Nie, J.Z. Jiang, Achieving large macroscopic compressive plastic deformation and work-hardening-like behavior in a monolithic bulk metallic glass by tailoring stress distribution, Appl. Phys. Lett. 92 (2008) 211905.

[18] S.H. Chen, K.C. Chan, F.F. Wu, L. Xia, Pronounced energy absorption capacity of cellular bulk metallic glasses, Appl. Phys. Lett. 104 (2014) 111907.

[19] P. Tandaiya, U. Ramamurty, R. Narasimhan, Mixed mode (I and II) crack tip fields in bulk metallic glasses, J. Mech. Phys. Solids 57 (2009) 1880-1897.

[20] P. Tandaiya, R. Narasimhan, U. Ramamurty, On the mechanism and the length scales involved in the ductile fracture of a bulk metallic glass, Acta Mater. 61 (2013) 1558-1570.

[21] R. Varadarajan, A.K. Thurston, J.J. Lewandowski, Increased toughness of zirconium-based bulk metallic glasses tested under mixed mode conditions, Metall. Mater. Trans. A 41A (2010) 149-158.

[22] S.H. Chen, A. Domel, T.M. Yue, C.P. Tsui, K.C. Chan, K.A. Dahmen, P.K. Liaw, Deformation behavior of bulk metallic glasses under a mixed-mode (I/II) loading condition, Intermetallics 93 (2018) 148-154.

[23] W.D. Li, Y.F. Gao, H.B. Bei, Instability analysis and free volume simulations of shear band directions and arrangements in notched metallic glasses, Sci. Rep. 6 (2016).

[24] R.T. Qu, M. Calin, J. Eckert, Z.F. Zhang, Metallic glasses: Notch-insensitive materials, Scr. Mater. 66 (2012) 733-736.

[25] R.T. Qu, J.X. Zhao, M. Stoica, J. Eckert, Z.F. Zhang, Macroscopic tensile plasticity of bulk metallic glass through designed artificial defects, Mater. Sci. Eng. A 534 (2012) 365-373.

[26] C.A. Schuh, T.G. Nieh, A nanoindentation study of serrated flow in bulk metallic glasses, Acta Mater. 51 (2003) 87-99.

[27] S.X. Song, H. Bei, J. Wadsworth, T.G. Nieh, Flow serration in a Zr-based bulk metallic glass in compression at low strain rates, Intermetallics 16 (2008) 813-818.

[28] K. Georgarakis, M. Aljerf, Y. Li, A. LeMoulec, F. Charlot, A.R. Yavari, K. Chornokhvostenko, E. Tabachnikova, G.A. Evangelakis, D.B. Miracle, A.L. Greer, T. Zhang, Shear band melting and serrated flow in metallic glasses, Appl. Phys. Lett. 93 (2008) 031907.

[29] K. Wang, T. Fujita, Y.Q. Zeng, N. Nishiyama, A. Inoue, M.W. Chen,

Micromechanisms of serrated flow in a $Ni_{50}Pd_{30}P_{20}$ bulk metallic glass with a large compression plasticity, Acta Mater. 56 (2008) 2834-2842.

[30] J.W. Qiao, Y. Zhang, P.K. Liaw, Serrated flow kinetics in a Zr-based bulk metallic glass, Intermetallics 18 (2010) 2057-2064.

[31] R. Sarmah, G. Ananthakrishna, B.A. Sun, W.H. Wang, Hidden order in serrated flow of metallic glasses, Acta Mater. 59 (2011) 4482-4493.

[32] G. Wang, K.C. Chan, L. Xia, P. Yu, J. Shen, W.H. Wang, Self-organized intermittent plastic flow in bulk metallic glasses, Acta Mater. 57 (2009) 6146-6155.

[33] B.A. Sun, H.B. Yu, W. Jiao, H.Y. Bai, D.Q. Zhao, W.H. Wang, Plasticity of ductile metallic glasses: A self-organized critical state, Phys. Rev. Lett. 105 (2010) 035501.

[34] J. Hu, B.A. Sun, Y. Yang, C.T. Liu, S. Pauly, Y.X. Weng, J. Eckert, Intrinsic versus extrinsic effects on serrated flow of bulk metallic glasses, Intermetallics 66 (2015) 31-39.

[35] H.B. Ke, B.A. Sun, C.T. Liu, Y. Yang, Effect of size and base-element on the jerky flow dynamics in metallic glass, Acta Mater. 63 (2014) 180-190.

[36] Z. Wang, J.W. Qiao, G. Wang, K.A. Dahmen, P.K. Liaw, Z.H. Wang, B.C. Wang, B.S. Xu, The mechanism of power-law scaling behavior by controlling shear bands in bulk metallic glass, Mater. Sci. Eng. A 639 (2015) 663-670.

[37] Y. Zhang, J.P. Liu, S.Y. Chen, X. Xie, P.K. Liaw, K.A. Dahmen, J.W. Qiao, Y.L. Wang, Serration and noise behaviors in materials, Prof. Mater. Sci. 90 (2017) 358-460.

[38] M.T.A. Khanouki, R. Tavakoli, H. Aashuri, J. Non Cryst. Solids 505 (2019) 62-71.

[39] S.H. Chen, K.C. Chan, L. Xia, Effect of stress gradient on the deformation behavior of a bulk metallic glass under uniaxial tension, Mater. Sci. Eng. A 574 (2013) 262-265.

[40] R.O. Ritchie, The conflicts between strength and toughness, Nat. Mater. 10 (2011) 817-822.

[41] R.T. Qu, J. Eckert, Z.F. Zhang, Tensile fracture criterion of metallic glass, J. Appl.

Phys. 109 (2011) 083544.

[42] A.L. Greer, Y.Q. Cheng, E. Ma, Shear bands in metallic glasses, Mater. Sci. Eng. R 74 (2013) 71-132.

[43] S. Adibi, P.S. Branicio, R. Liontas, D.Z. Chen, J.R. Greer, D.J. Srolovitz, S.P. Joshi, Surface roughness imparts tensile ductility to nanoscale metallic glasses, Extreme Mech. Lett. 5 (2015) 88-95.

[44] S.H. Chen, K.C. Chan, D.X. Han, L. Zhao, F.F. Wu, Programmable super elastic kirigami metallic glasses, Mater. Des. 169 (2019) 107687.

[45] S.H. Chen, H.Y. Cheng, K.C. Chan, G. Wang, Metallic glass structures for mechanical-energy-dissipation purpose: A review, Metals 8 (2018) 689.

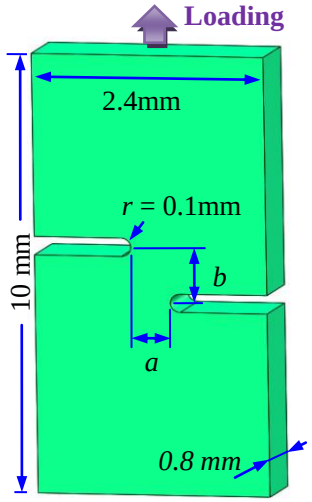

Three groups of specimens (**R**/**M**/**L**):

	a/mm	*b*/mm
R0:	0.4	0
R1:	0.4	0.4
R2:	0.4	0.6
R3:	0.4	0.8
M1:	0	0.4
M2:	0	0.6
M3:	0	0.8
L1:	-0.4	0.4
L2:	-0.4	0.6
L3:	-0.4	0.8

Figure 1. Schematic diagram showing the design of the reduced sections of the notched specimens with varying geometry parameters.

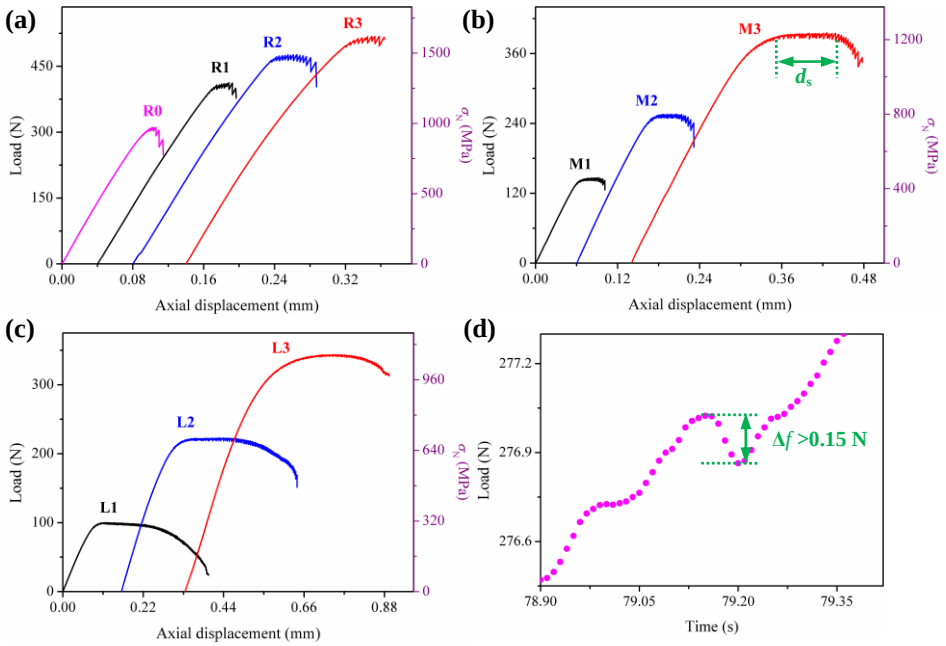

Figure 2. (a-c) Loading-axial displacement curves showing the plastic flows of the three groups of notched specimens, and (d) shows the occurrence of the first load drop with a magnitude larger than 0.15 N in **R0** specimen.

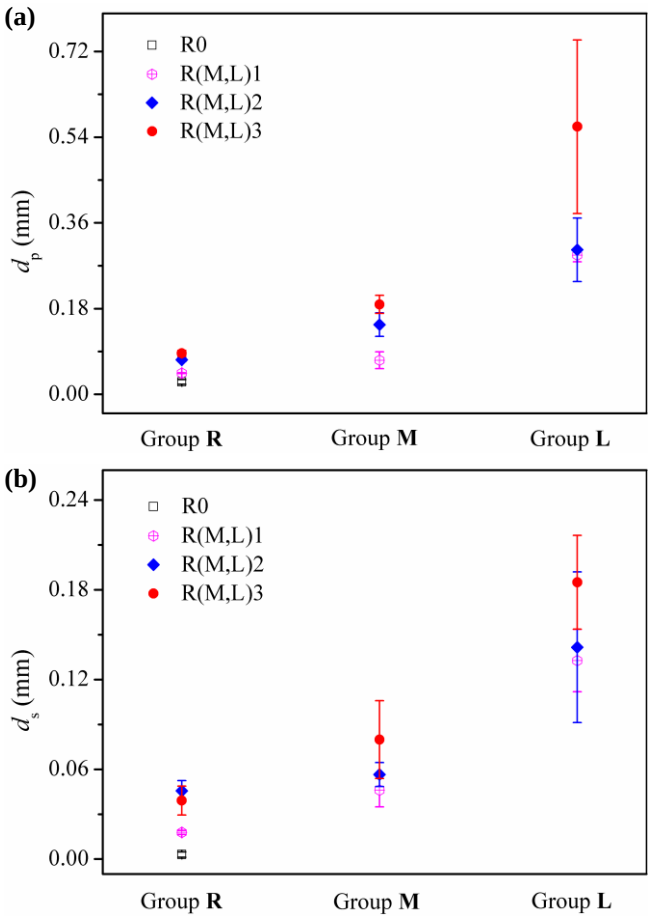

Figure 3. Plastic flow displacement (d_p) and the stable plastic flows (d_s) of the three groups of specimens.

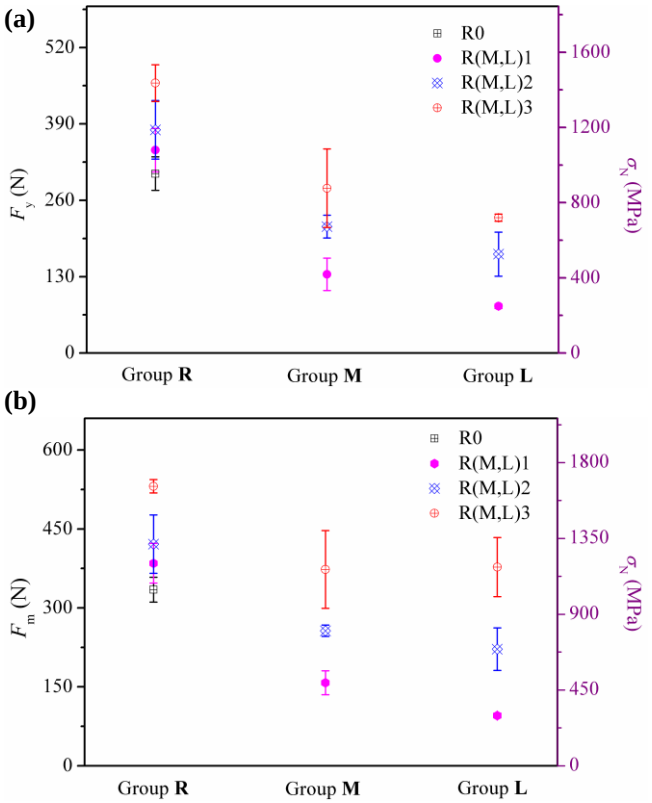

Figure 4. The "yield" load (F_y) and the maximum load (F_m) of the notched specimens.

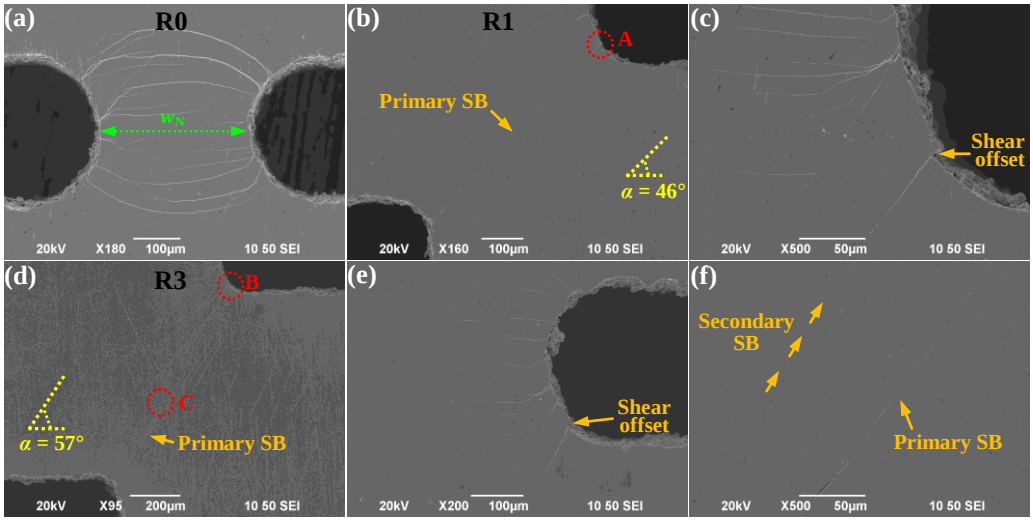

Figure 5. SEM images of the formation of shear bands in R0, R1 and R3 specimens, where (c), (e) and (f) are the magnified images at red circles A, B and C, respectively.

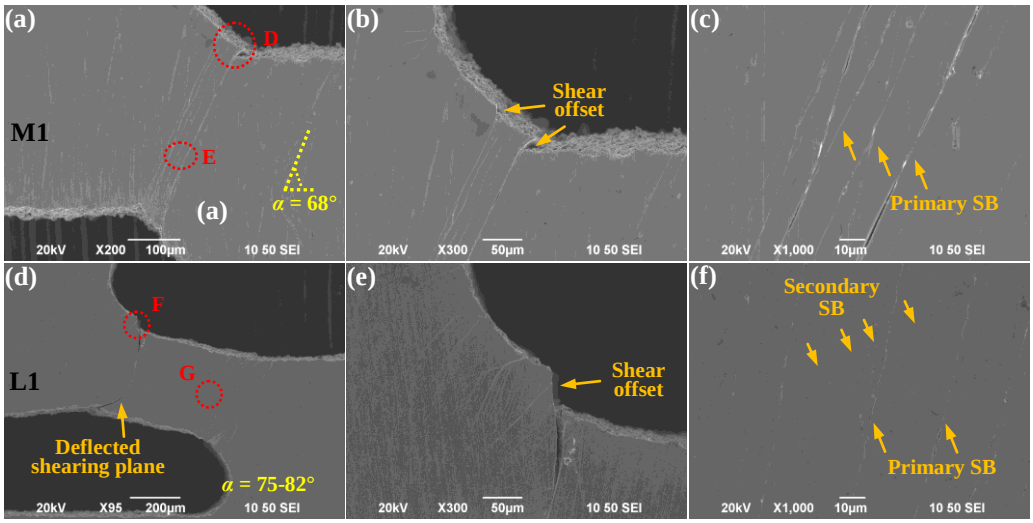

Figure 6. SEM images of the formation of shear bands in M1 and L1 specimens, where (b), (c), (e) and (f) are magnified images at red circles D, E, F and G, respectively.

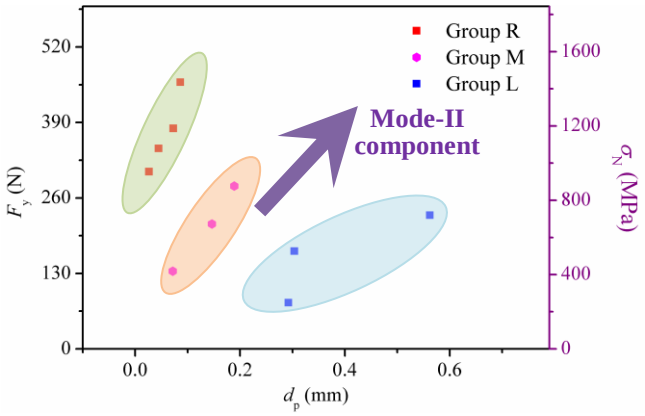

Figure 7. The increasing of plastic flows as well as bearing load in the notched BMG specimens under mixed-mode loading conditions